HiSST: 3rd International Conference on
High-Speed Vehicle Science & Technology
14-19 April 2024, Busan, Korea

A code-to-code comparison of turbulent hypersonic sharp cone-flares

Jimmy-John O.E. Hoste[1]
Tobias Ecker, Chiara Amato [2]
Nick Gibbons [3]
Doyle Knight [4]
Fahri Erinç Hizir, Tolga Köktürk [5]
Artemii Sattarov, Olivier Thiry [6]
Jean-Pierre Hickey [7]
Steven Qiang, Jim Coder [8]
Neil Castelino, Valerio Viti [9]

Abstract

As part of the AVT-352 on hypersonic turbulence, a code-to-code comparison has been initiated to evaluate the status of RANS modeling for such flows. To this end, two sharp cone-flare geometries, experimentally studied at CUBRC have been selected for study. Each geometry has been run at various conditions enabling a larger sampling for the various participating CFD codes and turbulence models. The nature of the physics found in cone-flare geometries is known to be extremely challenging for RANS CFD codes. This paper presents an initial status on this endeavor, describing the setups, conditions, and general simulating strategies. Initial simulations confirm the typical overpredictions of pressure and heat flux along the wall after the region of separation.

Keywords: *hypersonic, cone-flare, RANS*

1. Introduction

In order to advance the fundamental understanding of hypersonic flows, diverse experimental setups have been devised since the late 1950's [1]. The experiments aimed at isolating effects occurring on actual hypersonic vehicles and provide data to assess, validate, and further develop empirical correlation as well as numerical tools (CFD). An important focus of these experiments has been on shock-wave boundary-layer interactions (SWBLIs), both in laminar [2, 3, 4] and turbulent conditions [5, 6, 7]. Such

[1] *Destinus SA, Aerothermodynamics Branch, Switzerland, jimmyjohn.hoste@destinus.com*
[2] *DLR, Spacecraft Department, Göttingen, Germany*
[3] *Center for Hypersonics, University of Queensland, Brisbane, Australia*
[4] *Rutgers - The State University of New Jersey, New Brunswick, NJ 08903 USA*
[5] *Aselsan, Turkey*
[6] *Cadence Design Systems, Brussels, Belgium*
[7] *University of Waterloo, Canada*
[8] *The Pennsylvania State University, USA*
[9] *ANSYS Inc., 10 Cavendish Court, Lebanon, NH, 03766, USA*

interactions are typically found in control surface deflections, flared junctions, or intakes and require careful considerations in aerothermal design. A hypersonic vehicle, such as the National Aerospace Plane (NASP), is expected to encounter turbulent boundary layers in its flight path, as illustrated in Fig 1 of [8]. Specifically in the context of NASP, a set of experimental setups for shock wave turbulent boundary layer interactions (SWTBLI) was identified [9, 10] in order to guide the development of turbulence modeling in the context of CFD. An inventory of SWTBLI experiments as of 1994 was given by Settles and Dodson [8, 11] and a comprehensive survey of SWTBLI experiments, Direct Numerical Simulation (DNS) and Large Eddy Simulation (LES) as of 2023 was presented in Knight and Kianvashrad [12]. Settles and Dodson assessed the quality of existing datasets which would allow improving turbulence modeling. Among the type of setups, there was an axi-symmetric cylinder-flare which was introduced by Holden et al. [6, 7]. The motivation for a cone/flare type setup resulted from the desire to increase the complexity of SWTBLI's through crossflow effects while ensuring well-defined boundary conditions [6]. These early experiments were performed at Calspan's shock tunnel facilities, now commonly known as CUBRC facilities. Since then, many sets of experimental data on cone/flare interactions have been collected, including some more recent works performed in the last two decades [13, 14, 15, 16]. Moreover, Marvin *et al.* [17] provided a comprehensive experimental database for SWBLIs that includes baseline CFD solutions for the various test cases compiled.

SWBLIs have been the go-to type of test cases for validation of hypersonic CFD codes, driven by the desire to leverage numerical predictive capability in hypersonic vehicle design. In turbulent conditions, Reynolds-Averaged Navier-Stokes (RANS) modeling has always been the primary method of choice when engineering design is of interest. Anno 2024 this fact has (unfortunately) not changed, as the more accurate scale-resolving methods still remain out of reach for such purposes. Moreover, the availability of computational power at an affordable cost, as well as the advent of open-source CFD codes, allows whomever desires it to run (RANS) CFD test cases and obtain solutions in relatively short time frames. It is therefore more important than ever to focus on uncertainties in numerical predictions which can emanate from a CFD solver (numerical discretization and models) or its user (setup, meshing, modeling constant choices). In (turbulent) hypersonic CFD, wide prediction uncertainties have typically been encountered for SWBLI physics. This entails separation location, evolution of wall pressure, skin friction or heat flux including peak values. The latter set of quantities are key in the aero-thermal and -structural design of vehicles in the hypersonic regime and remain a challenge for RANS models.

Hypersonic cone/flare, hollow cylinder/flare and double-cone configurations have been popular for RANS code validations, as exemplified by [18, 19, 20, 21, 22, 23, 24, 25]. The interest varies from chemical and thermal non-equilibrium flow physics to laminar, transitional or fully turbulent flows. Such test cases have also been popular in blind validation of CFD codes [26, 27, 28, 29, 30]. These have typically been performed within the context of NATO Science and Technology Organization (STO) Applied Vehicle Technology (AVT) working groups [31, 30]. The present work similarly emanates from a NATO AVT group, the AVT-352 on hypersonic turbulence. Given the topic of interest, a RANS code-to-code validation has been initiated on hypersonic turbulent cone-flare geometries.

2. Problem Description

Two hypersonic turbulent cone-flare geometries, with experimental campaigns performed at various conditions, have been selected for code-to-code comparative studies amongst the participants. A first setup (Subsection 2.2) was experimentally studied at Mach 11 and 13 while the second setup (Subsection 2.3) at Mach numbers between 5 and 8, both with air as the working fluid. Both sets of experimental data have been obtained in the LENS' hypersonic facilities at CUBRC (reflected shock tunnels) [13, 17, 14]. In a first Subsection 2.1 the physics encountered in cone-flare like configurations are introduced followed by a description of the two test cases in Subsections 2.2 and 2.3, respectively.

2.1. Cone-flare related physics

The overall flowfield structure for a typical cone-flare configuration is shown in Figure 1 for CUBRC Run 28 at Mach 4.96 [32]. The forward cone half-angle is 7° and the aft flare angle is 40°. The streamlines are deflected by the attached incident conical shock[1]. A second bow shock is generated by the flare followed by a rapid expansion around the corner formed by the flare-cylinder junction. The incident shock-bow shock interaction occurs further downstream.

Details of the flowfield structure in the vicinity of the cone-flare junction are illustrated in Figure 2 for CUBRC Run 28 at Mach 4.96 [32]. The adverse pressure gradient due to the bow shock causes separation of the boundary layer on the cone surface and the formation of a separation region and shear layer. The deflection of the cone turbulent boundary layer by the separation streamline results in a separation shock which intersects the bow shock forming a triple point and transmitted shock. The surface pressure rises upstream of the separation point, achieves a plateau within the separation region, and rises again near the reattachment. The surface skin friction vanishes at the separation point, reverses direction within the separation region, and rises rapidly downstream of reattachment. Similarly, the surface heat transfer decreases within the separation region compared to the undisturbed boundary layer upstream, and rises rapidly immediately after reattachment.

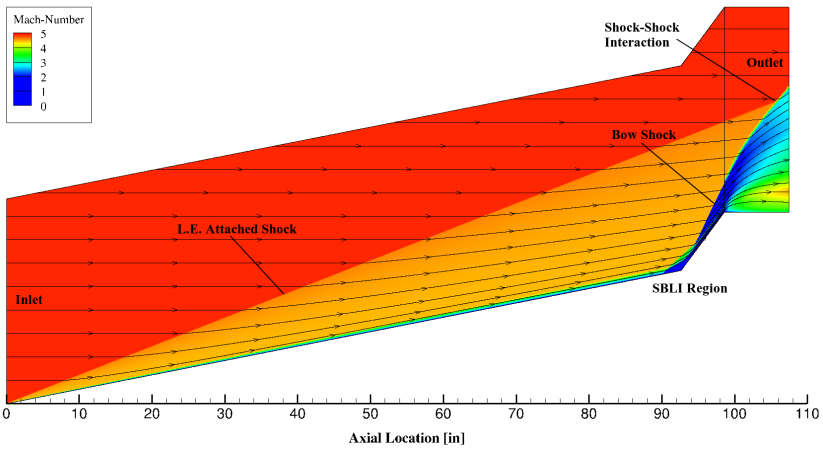

Fig 1. Overall flowfield structure CUBRC Run 28

[1]The half-cone angle for shock detachment at Mach 5 is 54.5°.

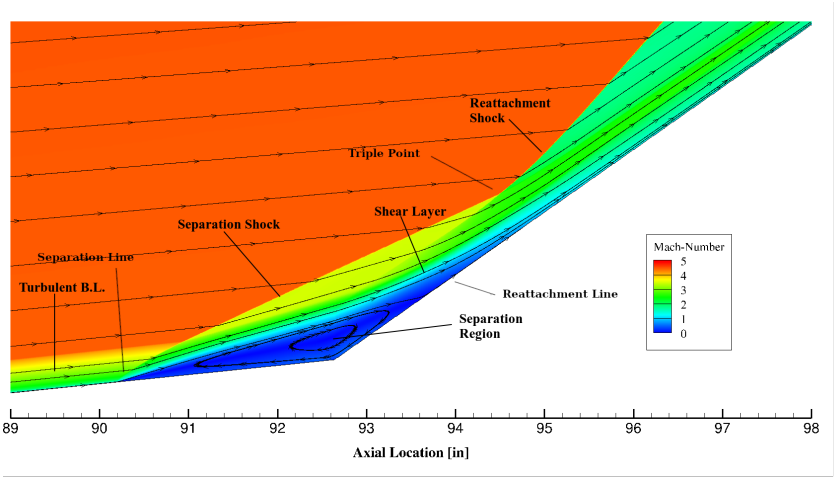

Fig 2. Details of flowfield structure CUBRC Run 28

2.2. Case 1: 6/42 Degree Cone-Flare at Mach 11 to 13

The first test case is a 6/42 degree large cone-flare as shown in Figure 3 and documented in [13, 17, 14, 15]. The flow conditions for two runs have been selected and listed in Table 1. The experimental data for Run 4 is tabulated in the following references [13, 17, 14]. Experimental accuracy on pressure and heat transfer measurements of ± 3 % and ± 5 %, respectively are reported in [17]. For Run 6, the experimental information can be found in [11].

Run number	Mach	ρ_∞ (kg/m^3)	T_∞ (K)	u_∞ (m/s)	p_∞ (Pa)	T_{wall} (K)
Run 4	11	0.032354	67.4	1807	626.07	300
Run 6	13.10	0.030952	57	1968	506.42	300

Table 1. Flow conditions of Run 4 [17] and Run 6 [11].

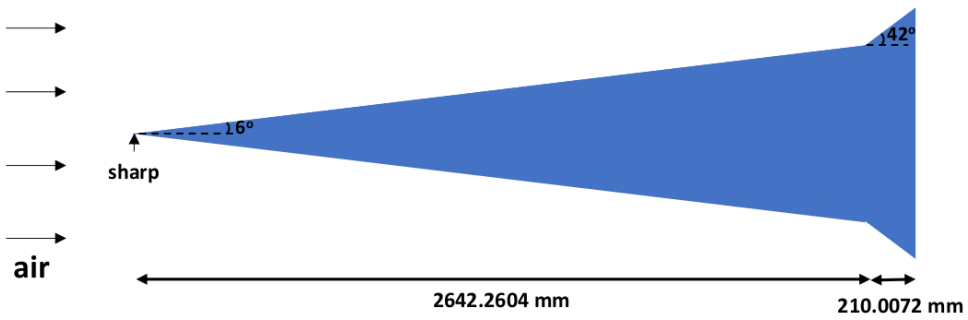

Fig 3. Cone-flare geometry used for conditions summarized in Table 1

2.3. Case 2: 7/40 Degree Cone-Flare at Mach 5 to 8

The second test case is a 7/40 degree large cone-flare as shown in Figure 4 and was part of a newer campaign for blind code validation [13]. The presently selected conditions of interest are runs with dry air, summarized in Table 2. Some of the experimental data has been presented in [14, 15] and is publicly available from the CUBRC website [2]. The length of the cone was devised to ensure transition occurs very close to the tip with transition locations reported by Holden *et al.* [14] (Table 22).

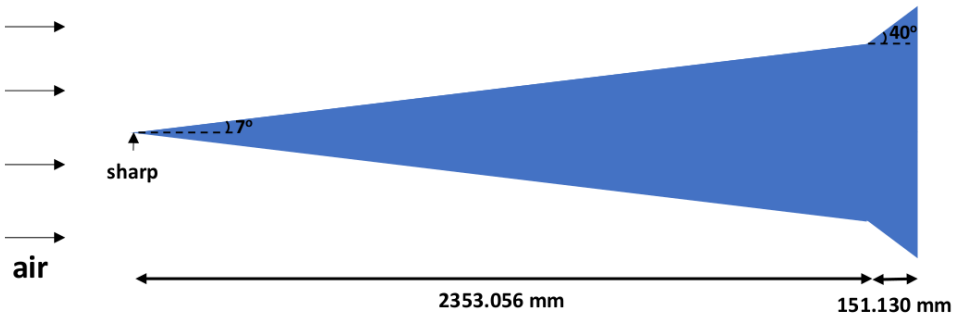

Fig 4. Cone-flare geometry used for conditions summarized in Table 2

Run number	Mach	ρ_∞ (kg/m^3)	T_∞ (K)	u_∞ (m/s)	p_∞ (Pa)	T_{wall} (K)
45	5.90	0.1113218	244.38	1852.0	7808	300
28	4.96	0.1417292	219.89	1476.5	8944	300
34	6.03	0.07112228	169.89	1578.1	3468	300
33	6.17	0.07369917	56.50	931.3	1195	300
14	7.18	0.05720705	66.61	1177.3	1094	300
41	8.10	0.02355281	166.94	2102.7	1128	300
37	8.21	0.04370412	60.44	1282.0	758	300

Table 2. Flow conditions for 7 / 40 cone-flare [14, 33].

3. Previous work and challenges for RANS

This section discusses previous attempts to simulate the setups described in Section 2 (see 3.1) as well as other relevant cases (see 3.2) where various RANS models have been adopted for predictive purposes. Finally, some RANS related developments specific to the physics encountered here are discussed in 3.3.

3.1. Hypersonic turbulent large cone-flare studies

3.1.1. 6/42 large cone-flare

Horstmann [34, 35] performed numerical validations on various hypersonic geometries, including the Mach 11 cone-flare case (Run 4). Various formulations of the k-ϵ model were used and behaved similarly

[2] https://www.cubrc.org/index.php/page/publications

in terms of wall pressure predictions. However, large discrepancies in heat flux predictions between the models, as well as with the experiments, were observed.

Holden et al. [13, 14] reports pressure and heat flux CFD data obtained with the DPLR code [36, 37] for Run 4 of Table 1. Simulations were performed with the k-ω SST (1994) [38] and an empirical shear-stress limiter coefficient (C_{lim}) following [39]. An optimal value for this coefficient of 0.9 was first found on the HiFIRE 1 (cone-cylinder-flare) setup and subsequently applied to Run 4. Separation onset was over-predicted by the model (CFD x $\approx$ 86 inches, experiment x $\approx$ 102 inches). The predicted peak heat flux and pressure values are similar to the experimental measurements, but their location further downstream.

Marvin *et al.* [17] reviewed a set of experimental setups relevant for SWTBLI CFD predictions. They provide a baseline CFD solution obtained with LAURA [40, 41] for Run 4 (see Table 1) of the 6/42 cone-flare geometry. This baseline prediction is obtained with the Wilcox' k-ω 2006 model and a compressibility correction with M_{t0}=0.5. It predicts very closely the onset of separation as seen by the pressure trace (CFD x $\approx$ 101 inches, experiment x $\approx$ 102 inches) as well as pre and post interaction heat flux and pressure values. Peak pressure and heat flux locations are accurately predicted, however, peak values are over-predicted. The baseline result follows from an extensive comparison between turbulence models by Gnoffo *et al.* [42]. Their work was motivated by NASA's Fundamental Aero Program (FAP) and aimed at reducing uncertainties in predictions of hypersonic flows by 50 %. Run 4 was used to compare multiple turbulence modeling approaches, adopting a calorically perfect gas model for air and relying on Sutherland's law for the molecular properties. The applied turbulence models were Cebeci-Smith, Baldwin-Lomax, Spalart-Allmaras, Menter's SST and the k-ω 2006. In general, the authors observe a strong grid sensitivity of the results. Specific study of the compressibility correction's impact on the k-ω 2006 model is reported with results demonstrating separation or not depending on its value. The k-ω 2006 model with M_{t0}=0.5 prove to be the best overall choice for this setup, as aforementioned.

More recently, Cross and West [25] used the commercial software Star-CCM+ to simulate the 6/42 cone-flare geometry for the Run 4 conditions with a structured grid. Menter's SST, Wilcox' k-ω 2006, Spalart-Allmaras and Realizable k-ϵ model were considered with strong variations in heat flux and pressure along the wall, including separation onset. A real-gas model in thermochemical equilibrium, implemented inside the solver is applied to represent the air. In a subsequent attempt, many variations of turbulence model parameters were explored, including the compressibility correction, the a_1 constant for the SST model (see also [43]) and the use of a quadratic constitutive relation (QCR, see Spalart [44]). A beneficial combination appears to be the omittance of the first, adapting the second parameter to 0.355 and to activate the QCR. This resulted in a separation onset predicted at x $\approx$ 100.4 inches (experiment x $\approx$ 102 inches).

3.1.2. 7/40 large cone-flare

This second geometry was originally considered as part of a blind code-to-code validation as explained by Holden [15, 14]. Candler [29] assessed the state-of-the-art in CFD for hypersonic flows. In this discussion, results for the aforementioned blind code-to-code validation at Run 45 conditions are presented. Strong variations in predictions, as expected, are observed. Results with Spalart-Allmaras (LAURA)

and SST from various codes (GASP, DPLR, US3D) are shown. In addition to uncertainties due to grids and numerical methods which have to be assessed to some extend, Candler points out the need for experimental uncertainty quantification which could be achieved by using the same geometry in multiple experimental facilities.

Holden *et al.* [45] briefly discusses additional results from the blind code-to-code validation for Run 28. In addition, the impact of wall temperatures is presented by comparing Run 33 and Run 45 results. Unfortunately, the graphs are of very low quality, making them difficult to read.

In a presentation, published on the CUBRC website, Wadhams *et al.* [46] presents results for Runs 28, 33, 45, 37 and 41 of Table 2 with the US CFD codes DPLR, FUN3D, US3D, GASP and LAURA. Most of the submissions were obtained with the SST turbulence model. For the two-equation turbulence models, peak pressures and heat fluxes on the flare are located in the vicinity of each other. This observation does not hold for the one-equation turbulence model results. Significant variations in predictions are observed for the different cases. Furthermore, the two-equation models have a tendency to predict separation onset in spite of experimental measurements indicating no likely incipient separation.

Alviani [33] studied the setup with Wilcox' k-ω 2006 version, reporting detailed results for run 28, run 34, run 33, run 14, run 41 and run 37. These simulation results will be considered in the present endevaour.

Cross and West [25] also considered the 7/40 degree cone-flare setup (Figure 4) for the conditions of Run 33 and Run 45 in their Star-CCM+ study. Simulations with both the Spalart-Allmaras and Menter's SST model are presented. For Run 33, the former turbulence model does predict a better separation onset (x $\approx$ 89.8 inches, experiment x $\approx$ 90.5 inches) as well as post-interaction values. In the separation zone itself, the heat flux is more appropriately predicted by Menter's SST model. Similarly, for the Run 45 comparison, the Spalart-Allmaras model predicts a better separation but flare heat flux values are underpredicted. Menter's SST overpredicts the flare heat flux values. Moreover, some sensitivity on the gas modeling assumptions is shown by comparing a single-species or two-species gas model.

Roy *et al.* studied this cone-flare configuration for the conditions of Run 37, Run 33 and Run 14 [47, 48]. They coupled the shock-unsteadiness model [49, 50] with Wilcox' k-ω turbulence model a variable turbulent Prandtl model which is active in shock regions. General improvements of heat flux predictions on the ramp are illustrated for all cases.

Other results found in the open literature include a presentation from Prabhu [51] which shows some sample results for Run 37 with DPLR and Menter's SST (ideal gas, Sutherland law, Prandtl = 0.71). Finally, Ali et al. [52] also simulated this cone-flare configuration for the conditions of Run 33 (dubbed Case-3), Run 14 (dubbed Case-2) and Run 37 (dubbed Case-1) listed in Table 2.They use a modified Spalart-Allmaras model which includes shock-unsteadiness (SU) related physics [50]. In comparison to the standard Spalar-Allmaras, the new model demonstrates a general improvement for the pressure traces (separation onset) but heat flux predictions remain challenging.

A summary of relevant simulation results from the literature for the cases and conditions presented in Subsections 2.2 and 2.3 are listed in Tables 3 and 4. The results are digitized from graphs and therefore prone to small errors. In some of the cases, no details on the CFD solver can be found. The same is true for the exact details of some of the turbulence models. For Run 6 and Run 34, no information could readily be found in the literature.

Table 5 summarizes the absolute variations between the various predictions compiled in Tables 3 and 4. It is clearly shown that even if variations in onset predictions are limited (at least for the 7/40 cone-flare geometry), variations in peak quantities are non-negligible. Relying on predictions would result in strong differences in thermo-structural design of such a geometry in practical applications.

3.2. Hypersonic turbulent RANS validation studies

In addition to the cone-flare geometry, discussed above, other canonical flow geometries have been used to validate RANS turbulence models [53, 11, 54, 35, 55]. Roy and Blottner [35] categorize seven canonical hypersonic flow setups, some of which have the relevant physical flow features of the cone-flare geometry. The two-dimensional compression corner and the cylinder flare share many of the characteristic features of the cone-flare, namely the pressure gradient and shock-boundary layer interaction. These flow features cause shock-induced flow separation, which is particularly challenging for RANS-based turbulence models. These challenges become even more important when heat flux is considered (see summary of results in [35]).

The impinging hypersonic shock has the benefit of isolating shock-induced boundary layer separation from the geometry of the flare setups. The experimental setups consist of a shock generator in the freestream above a fully turbulent hypersonic boundary layer. RANS investigations of this setup reveals that the velocity profiles are insensitive to the turbulence models but the eddy viscosity-based models uniformly overpredict the peak thermal loading [56]. This thermal loading error can be corrected by an anisotropic SST turbulence that accounts for the shock interaction physics [57].

More closely related to the cone flare is the two-dimensional compression corner. Wagner et al. [58] conducted a combined experimental and RANS-based numerical study on a heated compression corner with and without gap. The work highlighted the sensitivity of the transition location, and thus the characterization of the boundary layer, on the separation bubble, shock position, and maximum heat loading location.

The cylinder flare at a freestream Mach number of 7.05 [9]; this setup shares many of the same features as the conical flare studied herein. The RANS turbulence models studied by Zhang et al. [56] show significant variability peak pressure, heat load, and bubble separation size.

Many of RANS-based works rely on classical turbulence models and assumptions from low-speed equilibrium turbulence applications such as Boussinesq approximation or gradient-based molecular and turbulent diffusion models, the applicability of which in hypersonic conditions may be questionable [59]. A number of efforts have been underway to correct RANS models to better account for the particularlities of hypersonic flows. Some works have focused on developing strategies to account for variable turbulent

[1] not considering spike in heat flux similar to [33] probably linked to a spike in TKE
[2] hard to discern exact location but heat flux level correct
[3] Very hard to discern the exact location

Case	Run #	reference	CFD solver	Turbulence model	Separation onset (cm)	Peak pressure location (cm)	Peak pressure (kPa)	Peak heat flux location (cm)	Peak heat flux (MW/m^2)
6/42	4	[13, 14]	DPLR	k-ω SST 1994 (C_{lim} =0.9)	218.4	284.5	140.96	284.5	2.37
		[17]	LAURA	Wilcox' k-ω 2006 (M_{t0} = 0.5	256.5	268.4	173.00	268.2	4.73
		[25]	STAR-CCM+	k-ω SST 2003, a_1=0.355, QCR, no compressibility correction	255.0	270.8	158.80	270.7	3.79
	6	?							
7/40	45	[29, 46]	US3D	k-ω SST	230.9	240.9	273.20	240.7	4.86
		[29, 46]	DPLR (MacLean)	k-ω SST	233.0	239.1	256.90	238.2	4.34
		[29, 46]	DPLR (Prabhu)	k-ω SST	227.5	242.9	301.97	243.1	4.96
		[29, 46]	GASP	k-ω SST	230.8	240.9	276.98	240.6	5.42 [1]
		[29, 46]	LAURA	Spalart-Allmaras	234.8	238.7	248.58	248.2 [2]	2.81
		[25]	STAR-CCM+	k-ω SST 2003, a_1=0.355, QCR, no compressibility correction, 1-species air	231.2	240.1	274.52	239.9	5.24
		[25]	STAR-CCM+	Spalart-Allmaras, 1-species air	235.1	239.8	250.57	243.2	2.98
	28	[46]	US3D	k-ω SST	230.4	241.7	206.45	241.4	2.31
		[46]	DPLR (MacLean)	k-ω SST	232.4	239.4	209.40	238.7	2.29
		[46]	DPLR (Prabhu)	k-ω SST	230.3	242.7	202.82	241.8	2.24
		[46]	GASP	k-ω SST	229.4	242.6	210.36	242.1	2.54
		[46]	LAURA	Spalart-Allmaras	232.4	239.4	196.91	248.8	1.58
	34	?							
	14	[52]	?	Spalart-Allmaras	231.7	240.3	63.03	NA	NA
		[52]	?	Spalart-Allmaras SU	230.0	241.5	68.70	NA	NA
		[47, 48]	?	Wilcox k-ω SU	229.5	239.8	77.96	241.4	0.430
		[47, 48]	?	Wilcox k-ω SU and variable Pr_t	229.5	239.8	77.96	240.2	0.350

Table 3. Part 1. Quantities of interest from previous CFD studies of hypersonic turbulent cone-flares for conditions in Tables 1 and 2. Distances taken from the nose of the cone in the axial direction. Values prone to digitization errors.

Case	Run #	reference	CFD solver	Turbulence model	Separation onset (cm)	Peak pressure location (cm)	Peak pressure (kPa)	Peak heat flux location (cm)	Peak heat flux (MW/m^2)
7/40	33	[46]	US3D	k-ω SST	NIP	243.9	52.93	243.7	0.172
		[46]	DPLR (MacLean)	k-ω SST	229.9	239.9	46.09	239.6	0.175
		[46]	DPLR (Prabhu)	k-ω SST	226.1	243.2	51.73	242.8	0.183
		[46]	GASP	k-ω SST	NIP	244.3	52.22	243.7	0.192
		[46]	LAURA	Spalart-Allmaras	229.4	241.2	49.21	247.9	0.104
		[25]	STAR-CCM+	k-ω SST 2003, a_1=0.355, QCR, no compressibility correction	225.1	244.3	53.98	243.7	0.186
		[25]	STAR-CCM+	Spalart-Allmaras	228.1	241.9	52.92	243.1	0.113
		[52]	?	Spalart-Allmaras	229.3	242.7	50.91	NA	NA
		[52]	?	Spalart-Allmaras SU	229.8	242.1	50.25	NA	NA
		[47, 48]	?	Wilcox k-ω SU	229.1	240.8	49.19	240.8	0.170
		[47, 48]	?	Wilcox k-ω SU and variable Pr_t	229.1	240.8	49.19	240.8	0.135
	41	[46]	US3D	k-ω SST	228.8	242.0	96.33	241.8	3.00
		[46]	DPLR (MacLean)	k-ω SST	232.9	239.0	80.19	238.6	2.40
		[46]	DPLR (Prabhu)	k-ω SST	229.4	241.1	94.94	241.1	2.81
		[46]	GASP	k-ω SST	230.7	240.3	90.79	240.1	3.42
		[46]	LAURA	Spalart-Allmaras	234.8	239.2 [3]	80.41 [3]	242.6	1.42
	37	[46]	US3D	k-ω SST	226.6	242.7	73.26	242.6	0.787
		[46]	DPLR (MacLean)	k-ω SST	231.5 [3]	239.1	63.45	238.7	0.783
		[46]	DPLR (Prabhu)	k-ω SST	228.6	240.9	68.96	240.9	0.746
		[46]	GASP	k-ω SST	228.3	241.3	70.45	241.1	0.902
		[46]	LAURA	Spalart-Allmaras	232.6	238.9	59.98	243.4	0.420
		[52]	?	Spalart-Allmaras	234.4	239.6	56.35	241.7	0.539
		[52]	?	Spalart-Allmaras SU	230.7	240.8	66.72	246.4	0.608
		[47, 48]	?	Wilcox k-ω SU	231.1	240.1	61.85	239.9	0.950
		[47, 48]	?	Wilcox k-ω SU and variable Pr_t	231.1	240.1	61.85	239.9	0.766

Table 4. Part 2. Quantities of interest from previous CFD studies of hypersonic turbulent cone-flares for conditions in Tables 1 and 2. Distances taken from the nose of the cone in the axial direction. Values prone to digitization errors. NIP = not in picture, NA = not available.

Case	Run #	Δ Separation onset (cm)	Δ Peak pressure location (cm)	Δ Peak pressure (kPa)	Δ Peak heat flux location (cm)	Δ Peak heat flux (MW/m^2)
6/42	4	47.1	16.1	32.04	16.3	2.36
7/40	45	7.6	4.2	53.39	10.0	2.61
	28	3.0	3.3	13.45	10.1	0.96
	14	2.2	1.7	14.93	1.2	0.08
	33	4.8	4.4	7.89	8.3	0.088
	41	6.0	3.0	16.14	4.0	2.0
	37	7.8	3.8	16.91	7.7	0.53

Table 5. Absolute variations in predictions based on data available in the literature.

Prandtl numbers [60]. The focus on the turbulent Prandtl number is at the heart of the modeling strategy of Roy and Sinha [61] to improve the heat flux predictions in a compression corner. Other works have focused on the shock-turbulence interaction [59].

3.3. RANS models and developments applied to hypersonic flows

As pointed out in [62, 35, 29] turbulence modeling for compressible flows are adaptations from incompressible modeling by considering Favre averaging. These models are then applied to hypersonic flow studies. Compressibility corrections have been formulated [35, 29, 63] targeting various fluid dynamic phenomena. One of the widespread corrections relies on the turbulent Mach number to modify model coefficients in the destruction terms of the k-ω model [63]. It originates from Sarkar and Zeman's pressure-dilatation compressibility correction originally developed for free-shear flows. Rumsey [63] demonstrated the influence of the latter correction types on hypersonic boundary layers with significant variations between cold- and hot-wall cases and significant deviations from expected skin-friction and heat flux values. It is unclear whether they should be used or not. Sensitivity studies in hypersonic cone-flare geometries have also demonstrated such corrections to significantly impact the SWBLI behavior [42, 17, 25]. Tu et al. studied the effect of multiple compressibility corrections for the Spalart-Allmaras and SST models on two compression corners configurations with 15° and 34° deflection angles at Mach 9.22 [64]. The addition of the blended Catris's and Shur's compressibility correction is found to significantly improve the prediction of the SA model. Certain improvements in prediction have also been attained by adding Catris's correction to the SST model.

In various references discussed in Subsections 3.1 and 3.2, a key feature which RANS has difficulty to handle adequately, is the boundary layer recovery after separation. Coackley *et al.* [62, 65] investigated this issue for two-equation models in two-dimensional flows (flat plates and SWBLI). The baseline models were not able to predict reattachment heat transfer. Corrections to these models were investigated by the authors which involved modifications to algebraic length scale for the turbulent viscosity as well as rapid compression modifications or rapid strain corrections affecting damping functions and modeling constants

in the turbulence models, respectively. Improvements could be seen, but no conclusive modeling strategy, valid for all tested cases, could be devised.

Another common feature of RANS modeling for hypersonic flows is the use of a production limiter which effectively limits the ratio of production to destruction terms [42]. It targets specifically shock waves and the occurrence of unrealistically high values of TKE behind a shock. Canonical shock-turbulence interaction studies [66] have demonstrated some level of amplification of turbulence when passing through the shock. Actual amplitudes depend strongly on the shock strength, turbulence strength, and the nature of the turbulence itself. An example of unlimited predictions is shown by [33] with the Wilcox' k-ω turbulence model. An anomalous spike has been observed in heat transfer predictions for all the presented hypersonic cone-flare simulations. It has been linked to a strong increase in TKE at the exact same location. The same behavior has also been shown for the GASP predictions in [46] with Menter's SST model and can probably be related to this limiting.

Another method to deal with TKE amplifications through shock waves is to account for the actual physics governing the interaction. This is what Sinha *et al.* [49] have done by incorporating shock-unsteadiness into the k-ϵ turbulence model yielding clear improvements. In a subsequent work, Sinha *et al.* [50] extended the idea to SWBLI and applied it to one- and two-equation turbulence models. They apply the modeling to supersonic compression ramps and observe better prediction of separation onsets. However, post-ramp reattachment are delayed. The shock-unsteadiness (SU) model has not seen a widespread adoption in the hypersonic RANS community. For hypersonic cone-flare test cases, Ali *et al.* [52] showed some level of improvements by incorporating SU with a Spalart-Allmaras turbulence model. It is worth pointing out that a qualitatively similar effect to the SU model is present in Menter's SST 2003 model [67]. The model limits the turbulent viscosity based on the strain rate and the F2 blending function. As a result, in a shock, where S goes infinite, the eddy viscosity will be tend to zero in regions of the boundary layer where F2 is non-zero. As a result, production of TKE is strongly attenuated.

RANS modeling introduces various constants that have to be specified. Among these constants, the turbulent Prandtl number, introduced by modeling the Reynolds' heat flux term has shown to have some level of impact in predictions of supersonic combustors[68]. Moreover, a constant value of 0.89 is typically assume while it should vary spatially. In canonical shock-turbulence interaction, scale-resolving simulations have shown that the turbulent Prandtl number (Pr_t) reduces through a shock wave [69, 70]. Building on this observation, Roy *et al.* [61] have devised a variable Pr_t which is activated in shock regions through a shock function. They successfully demonstrated improvements in heat flux predictions in shock-generator type SWBLI cases as well as other hypersonic geometries [47, 48] including cone-flare setups. The shock-unsteadiness modified k-ω model with Pr_t following [48] has been applied by Ali et al. to Mach 9.22 2D wedge-compression corner cases revealing a drastic improvement of the heat flux prediction compared to the standard k-omega model [71]. The model validation has been performed for four 2D wedge-compression corner configurations with deflection angles from 15 to 38 degrees at Mach 9.22 as well as for the cases of Reynolds number variation and wall temperature variation.

Specifically related to Menter's (1994) SST model [38], Georgiadis and Yoder [43] demonstrate improved separation behavior and experimental agreement for SWTBLI by changing the a_1 constant, used in the turbulence viscosity evaluation, from 0.31 to 0.355. It is pointed by the authors that the recommendation's validity applies to the cases considered in their work (two SWTBLIs and HiFIRE 2) but no

generality can be ensured.

Some intrinsicalities of the present SWTBLI can't be represented through linear eddy viscosity models. Instead, non-linear eddy viscosity models (NLEVM), explicit algebraic Reynolds Stress Models (EARSM) or full Reynolds Stress Models (RSM) are required to account for the dominating anisotropies. This was already pointed out by Baurle [68] in an overview on the modeling for hypersonic propulsion flow paths in 2004. In recent years, some work [72, 73, 74, 57] has explored this area. Vemula and Sinha [72] explored three existing RSM to simulate the canonical homogeneous STI problem [66]. In general, the post-shock amplifications in the non-stream-wise directions were poorly captured by the models when compared to the DNS data. They then modify the Gerolymos *et al.* [75] model by introducing SU damping from [49]. This new model was able to correctly capture the canonical STI amplifications (for solenoidal incoming turbulence) for shock Mach numbers up to 6. Post-shock turbulence decay also shows improvements with respect to the unmodified model. In a subsequent work, Vemula and Sinha [74] explore the use of a SU modified EARSM. After demonstrating similar behavior to the SU modified RSM [72] for the canonical STI, the authors showed superior prediction with respect to other turbulence models on a two-dimensional SWBLI problem. Karl *et al.* introduced a correction for RSM, derived from the same canonical STI problem. They applied the correction on two RSM models retrieving the DNS behavior for the canonical STI. The model does still require further development as it violates Galilean invariance. Raje and Sinha [57] modified the SST model to account for anisotropies including SU physics. The new model, dubbed SUQ-SST, is applied to three two-dimensional SWTBLI configurations with some level of improvement in terms of separation onset and heat flux prediction with respect to the standard SST model [38] and similarly to better predictions with respect to a reference EARSM.

The various developments listed above have only been applied to a limited number of test cases. In order for a wider community to adopt new models, a larger set of validations is required, and if undesirable features are indentified, shielding modeling mechanisms should be devised. This problematic has also been pointed out by Roy and Blottner [35] and is key to advance the field of hypersonic RANS modeling.

4. Computational Setup

This section describes the general guidelines given to the participants (4.1) followed by a brief description of the CFD solvers and associated settings used.

4.1. General Approach

The aim of this endevaour is to establish anno 2023-2024, the capability of CFD solvers to simulate representative hypersonic flows with RANS approaches. A balance between commercial and research CFD codes (open-source and non open-source) have been adopted by the participants. Throughout the literature (see also 3), a general observation is the limited usage of commercial CFD softwares in simulating such hypersonic validation cases, or code-to-code comparison campaigns (GASP in[28] , GASPex in [30, 76, 22, 33] and StarCCM+ in [25]). Nevertheless, commercial codes are expected to play an important role in enabling a wider industrial community to perform hypersonic design tasks. This has become apparent in their development over the last years. It is therefore not surprising to see some of the participants to rely on commercial software.

Unlike typical code-to-code comparison studies, no mesh is provided nor any domain discretization approach imposed. Each participant is free to choose whichever computational domain and meshing strategy is most suited. An important requirement is to demonstrate grid independence. By allowing more freedom, the idea is to approach this comparison campaign from a more industrial / application-oriented perspective. It is up to the researcher / engineer to use their skills to the best of their capacity.

Participants are free to choose which RANS model to adopt, but it is encouraged to have at least a two-equation turbulence model. In the end, the aim is to assess the variation in predictions by comparing similar families of turbulence models.

4.2. Star-CCM+

In the current effort, with Star-CCM+ [77] version 2210, the desire was to step away from a structured grid approach described in [25] and instead rely on a strategy which would be feasible with any type of geometry, regardless of its complexity. This is achieved by using a combination of unstructured cells and a prism layer setup. In terms of prism layers, y^+ values below 3 were achieved by all meshes with the finer meshes ensuring values below 1 across both ramps. Grid sizes varied between 0.5M (coarsest) to 1M cells (finest).

The governing equations were solved in an implicit time stepping with inviscid fluxes treated with the AUSM+ flux-vector splitting. Discretization was ensured through a MUSCL third-order central-differencing treatment. Other solver settings were left their default values. Simulations were performed with a maximum CFL number of 1 which was an important requirement to converge the solutions in conjunction with the cell aspect ratios.

The two-dimensional axi-symmetric solver is selected in conjunction with Menter's SST 2003 turbulence model [67]. Following the detailed turbulence sensitivity study by Cross and West [25], the following turbulence solver settings were changed: usage of a quadratic constitutive relation (QCR) [44], deactivation of the compressiblity correction (turbulent Mach number based) and the modification of the a_1 model coefficient to 0.355 (default of 0.31) [43]. The working fluid, air, is treated as a thermally perfect gas.

4.3. TAU

DLR TAU is a hybrid structured/unstructured Navier-Stokes solver[78], which is validated for a wide range of steady and unsteady sub-, trans- and hypersonic flow cases. The TAU code is a second order finite-volume solver for the Euler and Navier-Stokes equations in the integral form using eddy-viscosity, Reynolds-stress or detached- and large eddy simulation for turbulence modeling. The AUSMDV[79] flux vector splitting scheme was applied together with MUSCL[80] gradient reconstruction to achieve second order spatial accuracy.

In order to determine required grid sizes a study on hybrid (unstructured / structured) grids generated by the Centaur mesh generator were used in conjunction with the Menter k-w SST turbulence model in the 2003 formulation[67]. The 2D grid sizes ranged from 100k points to about 800k points. Fine grids at about 600k points were needed to obtain the same heat flux slope. The first grid point was varied between 1e-3mm and 1e-4mm between the different grids, coarser first grid point spacing lead to overestimation of the heat fluxes. The use of QCR did not lead to any significant changes in the results.

Both the Thornber modification[81] as well as shock turbulence correction were used. For the gas model perfect gas with $gamma = 1.4$ and the appropriate Sutherland viscosity fit for air were used.

4.4. HyperCODA

The CFD solver framework HyperCODA [82, 83, 84] is the hypersonic extension to the flow solver CODA (CFD for ONERA, DLR, and Airbus), a next-generation CFD solver capable of solving large sparse linear systems derived from the implicit time integration of the RANS (Reynolds-averaged Navier-Stokes) equations with the assumption of a single perfect gas on three-dimensional structured and unstructured grids using either second-order finite-volume or higher-order Discontinuous-Galerkin (DG) discretization. This code has been internally developed at DLR to widen CODA applications from subsonic and transonic flow regimes to High Mach numbers flows, including non-ideal gas thermodynamics and gas mixture chemistry. The results shown in this paper are extensively presented in Amato et al. [85], where the authors explore HyperCODA capabilities and validate its accuracy in solving hypersonic flows around canonical hypersonic geometries, such as the 7°cone-40°flare test case.

This test case was solved using a two-dimensional grid, whose details and convergence study can be found in Amato et al. [85]. The flow was modeled as a single perfect gas using the Reynolds-averaged Navier-Stokes (RANS) equations in combination with the SA-negative turbulence model [86] and the AUSM+M [87] (Advection Upstream Splitting Method) convection scheme. The governing equations were solved using implicit time-stepping, and the chosen inflow conditions are the ones from RUN 45.

4.5. Eilmer

Eilmer is a open-source compressible flow simulation code developed at the University of Queensland for studying high-speed and hypersonic flow problems. [88] In this work Eilmer has been used to simulate nine of the experimental cases on both flow geometries, in 2D axisymmetric mode, using the production-limited, vorticity-source term, 2006 k-omega turbulence model (Wilcox2006-klim-V)[89], accelerated using a Newton-Krylov steady state solver [90]. The flow was modelled as a single-temperature, non-reacting, thermally perfect gas with temperature dependant specific heats, computed using the NASA Glenn Thermodynamic database [91]. The vorticity-based production version of the k-omega model was found to have better stability at high CFL numbers than its standard counterpart, though both produced similar results in terms of wall pressure and heat transfer.

4.6. GASP-ex

All details are provided in [33] with the most relevant information given below.

The axi-symmetric character of the experimental setup was used and quadrilateral structured grids generated. Grid sizes of 691 840, 2 616 960 and 10 167 040 cells are considered (2 nodes in the spanwise direction). Grid independence is demonstrated and the finest grid results are employed.

Inviscid fluxes are treated with a 3rd order ROE scheme and Min-Mod flux limiter for the reconstruction. Temporal integration is achieved through an inner-iterative Gauss-Seidel scheme. CFL numbers between 0.1 and 5 were adopted. Sutherland's law is adopted for both the dynamic viscosity and thermal conductivity. Wilcox' k-ω 2006 model is selected for turbulence modeling without any limiting or

compressibility correction.

4.7. Cadence Fidelity

Cadence's Fidelity is a CFD environment covering all the main CFD workflow stages, including geometry preparation, mesh generation, simulation, and, result analysis. In this study, Fidelity Hexpress mesh generator and Fidelity Flow density-based solver (DBS) are used.

An unstructured mesh is generated with Fidelity Hexpress. A surface-to-volume approach [92] is selected since it is a conventional approach for the aerospace industry thanks to its anisotropic surface meshing capabilities, which are particularly useful for aircraft leading and trailing edge meshing. In this approach, the surface mesh is generated as a first step, followed by the boundary layer extrusion, octree-based volume mesh generation, and reconnection between the boundary layer frozen surface and the volume mesh.

A 2D axisymmetric meshing strategy is used, with 1 cell in the third direction covering 2 degrees of the geometry and using the symmetry boundary conditions on the periodic boundaries. The mesh settings ensure a maximum y+ of around 1, an average y+ below 0.5, and a cell size in the shock region of 0.00125 m. A mesh sensitivity study comparing first off-wall cells sizes of 2.5E-6 m, 5E-7 m, and 1E-7 m revealed that it is necessary to keep the maximum y+ on the flare part around 1. The value of 5E-7 m is retained as an optimal value, ensuring sufficient grid convergence in terms of the first cell size. An approach with uniform refinement in the downstream shock region is employed due to its simplicity and ability to study multiple experimental setup operating points with different Mach angles. The total cell count is equal to 603 983 cells. An optimal mesh based on a tailored refinement box following the shock and recirculation regions or solution-based adaptive remeshing can be used to drastically reduce the cell count.

The Fidelity Flow solver is employed with a density-based formulation (DBS) to solve the governing system of equations for flow and turbulence. The flow solver applies a cell-centered finite volume method with local time-stepping for the integration of the governing flow equations. The convergence is accelerated by using the in-house CPU Booster technique and geometric multigrid techniques. Several spatial discretization techniques are available, namely the second-order central Jameson, Schmidt, and Turkel scheme with scalar and matrix dissipation formulations, Roe-type upwind scheme, and AUSM-type Low-Diffusive Flux Splitting Scheme (LDFSS). Pseudo-time integration is performed using an explicit multi-stage Runge–Kutta scheme. The solver features multiple Reynolds Averaged Navier-Stokes (RANS) turbulence models together with more advanced Large Eddy Simulation and hybrid RANS/LES models. The turbulent heat flux vector is modeled by introducing a turbulent thermal conductivity connected to the eddy-viscosity through a turbulent Prandtl number.

The results presented in this paper are obtained using the second-order LDFSS scheme, Menter's SST 2003 with the a1 coefficient set to 0.355, SBSL-EARSM, and SSC-EARSM [93] turbulence models, a single-temperature non-reacting gas model based on viscosity, thermal conductivity and specific heat capacity properties as a function of temperature following Lemmon [94], and Turbulent Prandtl number set to 0.86 following the literature review done in [35] and experimental measurements in supersonic flows by Van Driest [95].

4.8. Ansys Fluent (Aselsan)

Two-dimensional axi-symmetric simulations are performed with a structured quadrilateral and unstructured combined quadrilateral and triangular mesh, for the first (Subsection 2.2) and second case (Subsection 2.3), respectively. Present simulations were run on grids generated with ICEM CFD for the former case and Ansys Meshing software for the second case. Grid sizes between 1 M and 19M cells were used for the first geometry. For the second geometry, a pressure-gradient and density-gradient mesh adaptation was used to limit the cell count resulting in grid sizes between 0.4 and 0.8 M cells. Results presented herein are obtained on a 10 M and 0.8 M element grid for the former and second geometry, respectively. Values of y^+ below 1 were ensured on both grids. Thermally perfect gas assumptions are adopted. The density-based solver is utilized with an implicit formulation and inviscid fluxes are treated with an AUSM+ flux-vector splitting scheme in Ansys Fluent 2021 R2 for Run 4 (Table 1). The pressure-based coupled solver in Ansys Fluent 2021 R1 is used for Run 45 (Table 2). The Green-Gauss Node Based method is applied for gradient reconstruction and second-order (upwind) spatial discretization is employed for both cases. A steady-state formulation is adopted. The freestream turbulence parameters were set at a turbulence intensity of 1% and turbulence viscosity ratio of 1 for Run 4. Values of 5 % and 10 were used for the same parameters in the Run 45 simulations. Note that insignifcant changes were observed by prescribing 1 % and 1 in Run 45 for these freestream quantities. Predictions with the k-ω SST model are currently presented but simulations with Spalart-Allmaras as well as thermal non-equlibrium models have been performed.

4.9. SU2

SU2 is an open-source computational analysis suite for the solution of the Navier-Stokes equations and other partial differential equations in computational physics [96]. It has a broad user base in computational physics, with a strong emphasis in aerospace, and recent developments have added capabilities in non-equilibrium thermodynamics for applications in high-Mach number flows [97]. Despite the relevance of these advances to the present work, the classical equilibrium thermodynamic model–but with variable thermophysical properties–is used herein in order to explore the various turbulence modeling approaches.

Both a two-dimensional axisymmetric and a quasi-three dimensional mesh are generated in Pointwise (18.4) using wall-normal extrusion layers. Three meshes with increasing resolution of about 125,000, 327,000, and 725,000 grid points are investigated; the y^+ is maintained below unity for the medium and fine cases, although the wall resolution is not maintained for the coarsest mesh. The simulations are run in SU2 (Harrier 8.01), primarily with the k-ω SST turbulence model (2003 version). The AUSM convective scheme is used with a Venkatakrishnan slope limiter.

4.10. OVERFLOW

OVERFLOW is a three-dimensional, structured, overset CFD solver developed at NASA for various flow problems. In this work, OVERFLOW version 2.4b was used with the HLLE++ upwinding scheme with SSOR to handle the inviscid fluxes. The 2D structured meshes were generated using the Pointwise®mesh generation software. The mesh was generated as a 2D axisymmetric mesh with an initial $y+$ of 0.5, and solved with the SA turbulence model.

4.11. Ansys Fluent (Ansys Inc.)

For this study, we utilize a 2D axisymmetric structured quad mesh in the commercial CFD code Ansys Fluent. The grid is created using Ansys SpaceClaim Mesher, and it is designed so that the cells in the boundary layer have a y^+ below 1. The Fluent solver offers the option to solve the Navier Stokes equations using either a pressure-based implicit solver (PBNS) [98, 99] or a density-based implicit or explicit solver (DBNS) [100, 101], either in steady-state or unsteady mode. The present case is solved using the coupled steady-state DBNS solver. An Implicit, Roe Forward-Difference-Scheme (Roe-FDS) was used for the calculation of the convective fluxes. A second-order upwind spatial discretization is achieved using the Green-Gauss Node Based (GGNB) gradient formulation. High Speed Numerics (HSN), High-order Term Relaxation and Convergence Acceleration for Stretched Meshes (CASM) were used to improve convergence. Run 14 and Run 45 are simulated using ideal gas air. Kinetic theory and Sutherland's model are used for calculating thermal conductivity and viscosity, respectively. Turbulence is modelled using a Generalized K-Omega (GEKO) model [102]. GEKO is based on the K-Omega formulation and provides users with four free parameters which can be adjusted over a wide range of applications. For Run 45, Coefficient of Separation (C SEP) is set to 0.9 due to late separation predictions. Each run was initialized from the pressure far-field followed by a FAS Multigrid initialization.

5. Results and Discussion

This section presents some of the results already obtained by the participants. It must be noted that not all results are definitive; some are subject to improvements along the validation endeavour.

5.1. 6/42 cone-flare

Figure 5 shows the wall pressure and wall heat flux predicted by four of the participants with CFD codes STAR-CCM+, Eilmer, Ansys Fluent and SU2. Note that, as pointed out in [42, 17], the experimental data x-locations are taken along the cone ramp and have to be transformed to represent positions with the x-axis aligned with the symmetry axis of the cone-flare geometry. All simulations are predicted with a k-ω type of model, Wilcox' 2006 for Eilmer and a version of Menter's SST for the others. Variations of separation onset of 9 cm are observed. The STAR-CCM+ results, with modified turbulence modeling settings (see 4.2), predict the correctly the separation onset for this setup and condition. The STAR-CCM+ traces do show some oscillations on the ramp which is attributed to the grid variation between the cone and the flare in the vicinity of the shock-shock interactions. A similar numerical artefact has been reported by Cross and West [25] for the same solver. All simulations overestimate the experimental peak pressure and heat flux values values. This observation is commonly seen in the literature.

5.2. 7/40 cone-flare

Figure 6 shows the wall pressure and wall heat flux traces obtained by three commercial softwares (GASPex, Ansys Fluent and STAR-CCM+) and two open-source codes (Eilmer and SU2). Variations in separation onset of 4 cm are found and the correct separation behavior is predicted by Ansys Fluent and the GEKO turbulence model (see 4.11). Experimental peak pressure values are not over-estimated by the solvers but the location varies significantly. However, peak heat flux predictions are still over-predicted by all solvers with values of the same order of magnitude. Like for the 6/42 cone-flare geometry (see 5.1), STAR-CCM+ is characterized by numerically induced oscillations in the wall predictions on the flare.

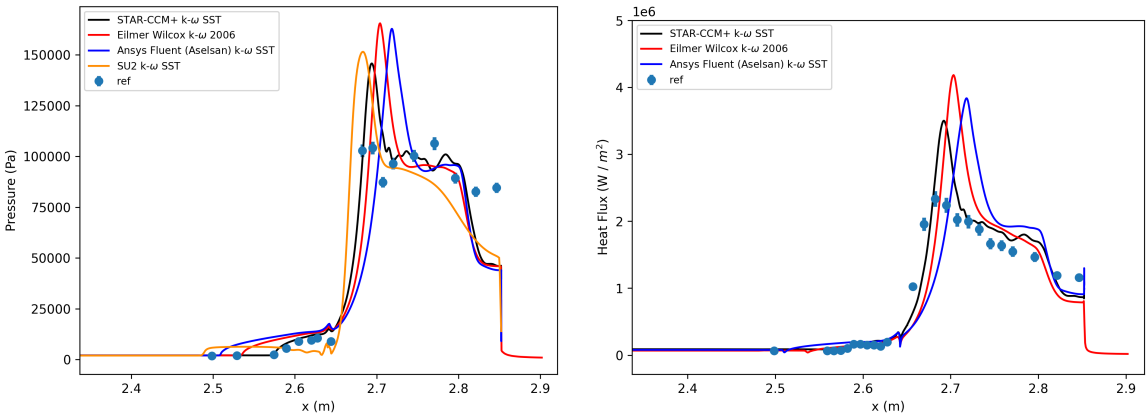

(c) (d)

Fig 5. Traces of wall (a) pressure and (b) heat flux obtained for Run 4 with k-ω type turbulence models.

GASPex heat flux traces show a spike at the cone-flare interface which was linked to a jump in TKE [33]. A similar effect with the same solver has been reported in the literature [46]. A possible remedy in the turbulence modeling would be the use of a production limiter.

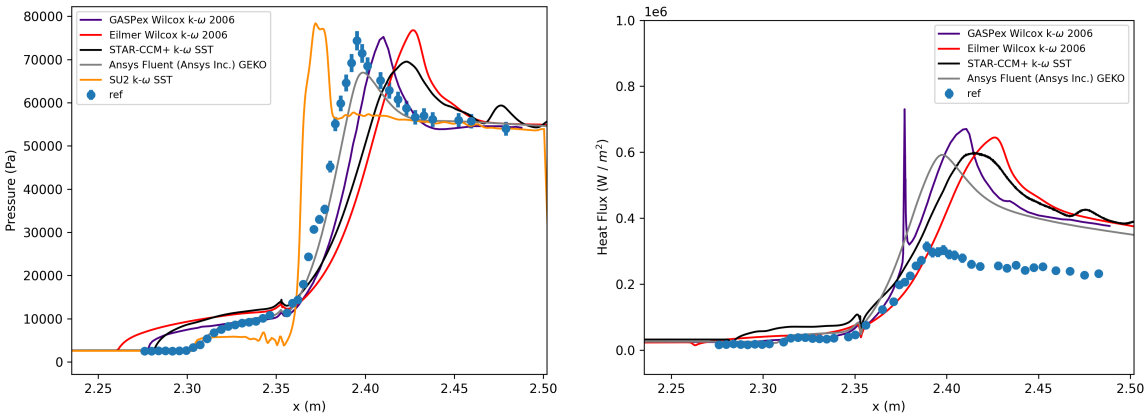

(c) (d)

Fig 6. Traces of wall (a) pressure and (b) heat flux obtained for Run 14 with k-ω type turbulence models.

Run 45 for this second cone-flare geometry has been run by most of the participants, yielding a larger pool for predictive uncertainty evaluation. In a first comparison, the nose heat flux is given in Figure 7. The experimental heat flux data illustrates the rapid transition to a turbulence state. Generally, the different turbulence models and solver predict values within experimental observations. Only the Eilmer results with Wilcox k-ω 2006 tend to underpredict the cone heat flux for this condition. The various SST models are predicting similar levels of heat flux. Note that the experimental data points do indicate some (oscillatory) variation in heat flux level. These fluctuations are most probably linked to

the experimental setup and data acquisition apparatus and not due to fluid dynamic phenomena [3]. Some of the predictions indicate some spurious fluctuations with STAR-CCM+ having the largest amplitudes. The reason for this is attributed to the mesh misalignment with the shock as well as the difficulty of the solver in dealing with large cell aspect ratios at the wall. The latter is unfortunately important in order to limit the grid sizes for such geometries.

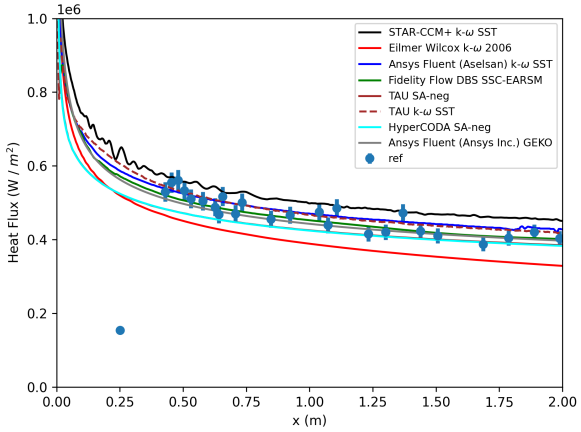

Fig 7. Heat flux predicted by various solvers on the cone for Run 45

Figures 8, 9 and 10 compare the wall pressure and heat flux traces at the cone-flare junction with some variations between the different turbulence modeling approaches and solvers. The two-equation models (Figure 8) tend to predict larger separation bubbles which in turn results in peak heat flux prediction locations further downstream on the flare geometry. Except for STAR-CCM+, the peak heat flux values are of the same order of magnitude as the experimentally measured one.

The HyperCODA, and TAU, solution obtained with the SA-negative turbulence model underpredicts the wall heat flux in the zone of interest with respect to the experimental data and the other solutions obtained with the k-ω turbulence models. While HyperCODA is still under development, this behavior was expected and already observed in [15, 25], showing that SA turbulence models predict a smaller separated region, an attached flow in the corner, and a lower peak of the wall heat flux. Furthermore, using a well-established code like TAU with RANS-SAneg and AUSM+M convection scheme, the predicted heat flux coincides almost exactly with the HyperCODA solution, proving that the underprediction is a direct effect of the chosen turbulent model. On the other hand, as it can be seen from Fig.8, the HyperCODA pressure is in good agreement with the experiments, besides the peak corresponding to the separation region, not forecasted by HyperCODA. The experimental Schlieren for this run condition do not indicate separation as pointed out in [46]. Most of the predictions do over-estimate the separation bubble. Figure 10 illustrates the results for what could be considered more advanced turbulence models which have seen their developments in the past decade.

Multiple sensitivity studies have been performed in Fidelity Flow DBS to study sensitivity to the mesh resolution, constant turbulent Prandtl number values, numerical schemes, and gas modeling techniques. Figure 11 presents the sensitivity analysis related to the turbulence modeling approach. Menter's SST

[3]Private communication with Alexander Wagner (DLR).

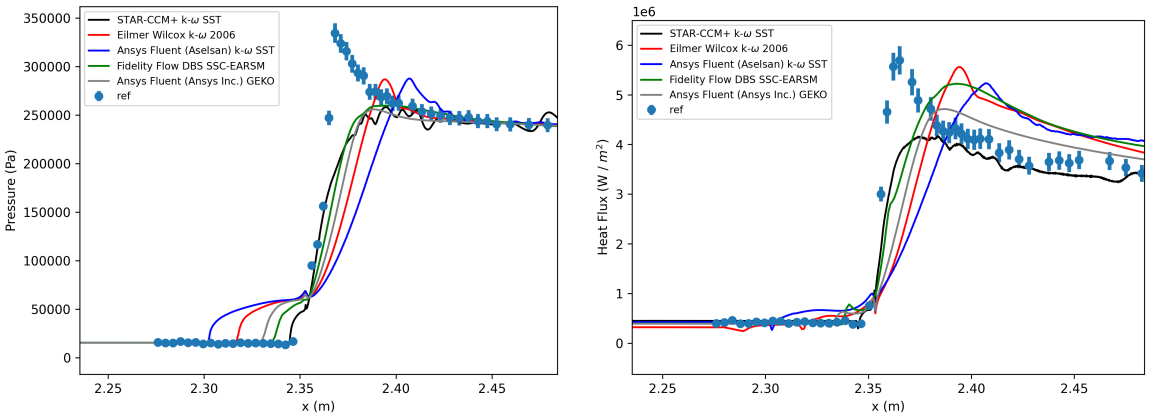

(c) (d)

Fig 8. Traces of wall (a) pressure and (b) heat flux obtained for Run 45 with various two-equation turbulence models.

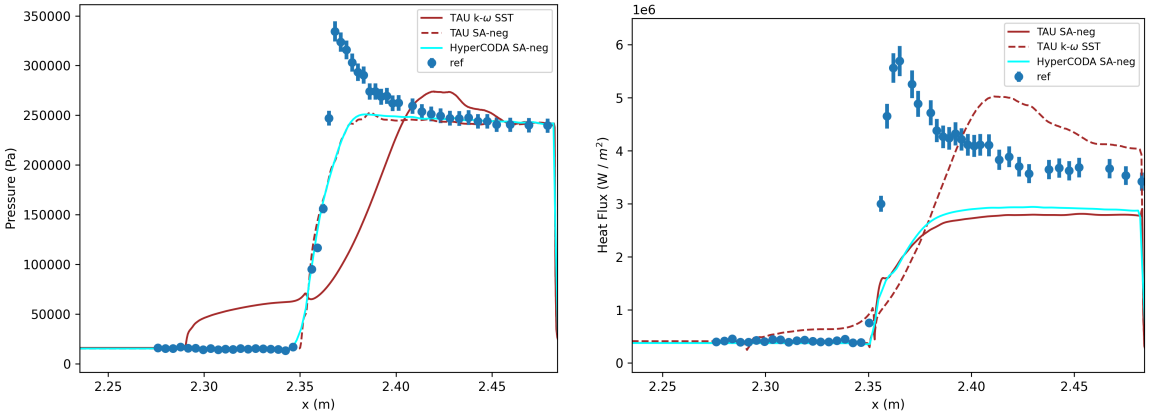

(c) (d)

Fig 9. Traces of wall (a) pressure and (b) heat flux obtained for Run 45 with TAU and HyperCODA.

2003 with the a1 coefficient set to 0.355, SBSL-EARSM, and SSC-EARSM turbulence models are compared in terms of heat flux and static pressure prediction. The heat flux comparison on the cone part reveals that all the models predict the trend that agrees with the experimental data in the turbulent flow region, with the SSC-EARSM model having the smallest deviation from the experimental data. Such improvement in prediction over the SST and SBSL-EARSM models can be attributed to the improved near-wall behavior of the turbulence energy thanks to the function introduced to damp the turbulence energy destruction close to the wall [93]. The analysis of the obtained turbulent kinetic energy field confirms that SSC-EARSM model predicts higher values of the turbulent kinetic energy downstream of the shock and in the boundary layer compared to the SBSL-EARSM model. The heat flux prediction on the flare part obtained with the SSC-EARSM model is significantly closer to the experimental data compared to the SBSL-EARSM model. The SSC-EARSM turbulence model predicts the highest maximum peak pressure value. The maximum static pressure predicted by the SST and SBSL-EARSM models is 5.4%

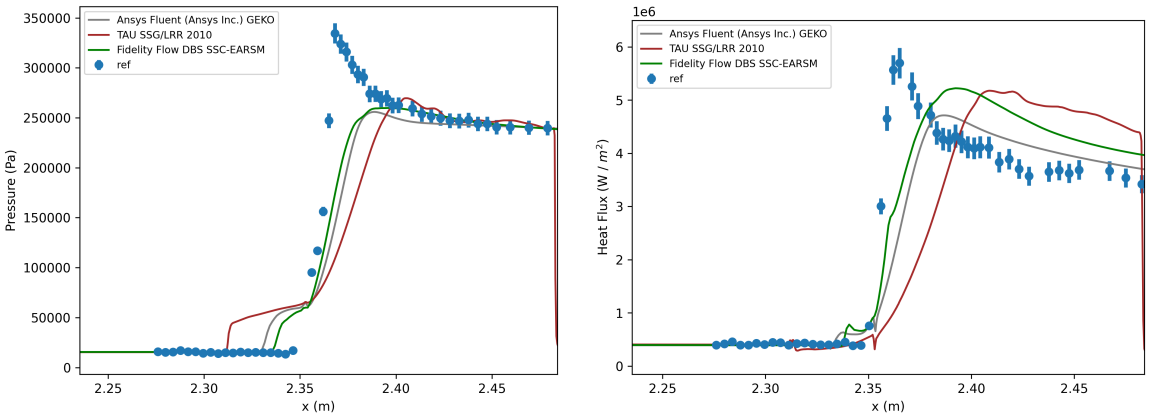

(c) (d)

Fig 10. Traces of wall (a) pressure and (b) heat flux obtained for Run 45 with more recent turbulence model.

and 2.3% lower correspondingly compared to the SSC-EARSM value. A small or no corner separation region is predicted by Fidelity Flow DBS with the three employed turbulence models.

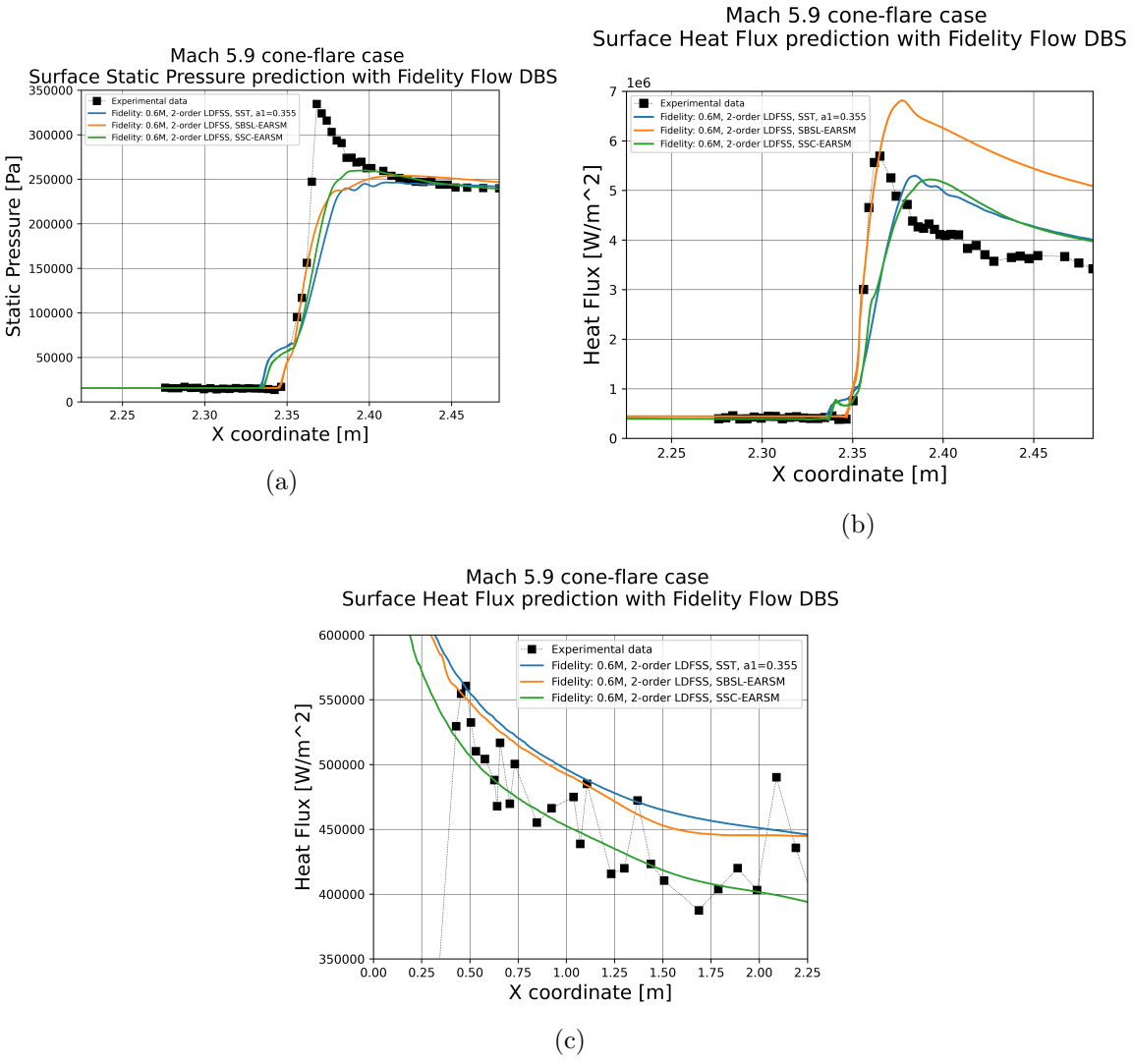

Fig 11. Traces of wall (a) pressure and (b), (c) heat flux obtained with Cadence's Fidelity Flow DBS for Run 45 with k-ω SST, SBSL-EARSM, and SSC-EARSM.

6. Conclusions

In this work, an extensive review of the literature on RANS simulations of hypersonic turbulent flow over sharp cone-flares has been performed. Numerical studies of such geometries have typically been motivated by CFD code validations and have been popular in (blind) code-to-code comparisons. The axi-symmetric configuration allows for the isolated study of shock wave turbulent boundary layer interactions with cross-flow effects. The large cone ensures that a turbulent boundary layer develops prior to the cone-flare junction. Multiple sets of experimental data are publicly available for such geometries with different cone and flare angles. Measurements include pressure and heat flux traces along the wall as well as Schlieren visualizations. Accurate and reliable predictions for sharp cone-flare geometries, as well as other similar hypersonic canonical configurations, are known to be challenging for CFD codes and RANS methods. Simulations typically fail in correctly predicting boundary layer separation and strongly over-predict the heat flux on the flare. The various historical developments of RANS modeling, relevant to these hypersonics configurations, have been discussed. These vary from various compressibility corrections to additional modeling terms based on shock-turbulence physics from canonical DNS studies. Unfortunately, the need for case-dependent tuning is typically reported in the literature. A promising approach with regard to improved predictions of turbulent shock wave boundary layer interactions is the variation of the turbulent Prandtl number. It is typically set as a constant but it does vary across shock waves and accounting for this fact has resulted in less over-predictions of heat flux levels on the flare. However, the latter modeling strategy has not yet been adopted in the larger hypersonic RANS community.

In general, significant variations in the predictive capability of CFD codes for hypersonic turbulent large cone-flare geometries has been observed. As part of the AVT-352 on hypersonic turbulence, we wish to assess the current uncertainty in simulating such test cases. In this work we select two geometries, available in the literature, for which experimental measurements have been collected at various flow conditions. This work presents a summary of the test cases and the run conditions of interest, as well as the general simulation strategy. A large pool of participants, working with different CFD codes, has been gathered in order to contribute with numerical simulations of the test setups. This also includes more recent turbulence modeling approaches. Preliminary simulations confirm the typical observations found in the literature.

Acknowledgements

The first author would like to thank Robert A. Baurle (NASA Langley) for the valuable advice provided during this work. The first author would also like to thank Alexander Wagner (DLR Göttingen) for the insight provided on boundary layer transition in reflected shock tunnel experiments.

References

[1] M Holden. Historical review of experimental studies and prediction methods to describe laminar and turbulent shock wave/boundary layer interactions in hypersonic flows. In *44th AIAA Aerospace Sciences Meeting and Exhibit*, page 494, 2006.

[2] MS Holden. Experimental studies of separated flows at hypersonic speeds. ii-two-dimensional wedge separated flow studies. *AIAA Journal*, 4(5):790–799, 1966.

[3] MS Holden. Experimental studies of separated flows at hypersonic speeds. i-separated flows over axisymmetric spiked bodies. *AIAA Journal*, 4(4):591–599, 1966.

[4] MS Holden. Theoretical and experimental studies of the shock wave-boundary layer interaction on compression surfaces in hypersonic flow. Technical report, Cornell Aeronautical Lab Inc Buffalo NY, 1970.

[5] MS Holden. Shock wave-turbulent boundary layer interaction in hypersonic flow. Technical Report ARL TR 75-0204, Calspan Corporation, 1975.

[6] M Holden. Experimental studies of quasi-two-dimensional and three-dimensional viscous interaction regions induced by skewed-shock and swept-shock boundary layer interaction. Technical Report 7018.A-2, Calspan Advance Technology Center, 1984.

[7] MS Holden, AG Havener, and CH Lee. Shock wave/turbulent boundary layer interaction in high-reynolds-number hypersonic flows. Technical report, CALSPAN UB RESEARCH CENTER BUFFALO NY, 1987.

[8] GS Settles and LJ Dodson. Supersonic and hypersonic shock/boundary-layer interaction database. *AIAA journal*, 32(7):1377–1383, 1994.

[9] M Kussoy, L Levy, and F Menter. Hypersonic flows as related to the national aerospace plane. Technical Report NACA-CR-187985, NASA, 1991.

[10] M Kussoy, GPG Huang, and F Menter. Hypersonic flows as related to the national aerospace plane. Technical Report NACA-CR-199365, NASA, 1995.

[11] GS Settles and LJ Dodson. Hypersonic shock boundary-layer interaction databse. Technical Report NACA-CR-177577, NASA, 1991.

[12] D Knight and N Kianvashrad. *Hypersonic Shock Wave Turbulent Boundary Layers - Direct Numerical Simulation, Large Eddy Simulation and Experiment*. Institute of Physics, Bristol, United Kingdom, 2023.

[13] M Holden, T Wadhams, M MacLean, and E Mundy. Experimental studies of shock wave/turbulent boundary layer interaction in high reynolds number supersonic and hypersonic flows to evaluate the performance of cfd codes. In *40th fluid dynamics conference and exhibit*, page 4468, 2010.

[14] MS Holden, TP Wadhams, and MG MacLean. Measurements in regions of shock wave/turbulent boundary layer interaction from mach 4 to 10 for open and "blind" code evaluation/validation. In *21st AIAA Computational Fluid Dynamics Conference*, page 2836, 2013.

[15] M Holden, T Wadhams, M MacLean, and A DuFrene. Measurements in regions of shock wave turbulent boundary layer interaction from mach 3 to mach 10 for open and blind code evaluation validation. Technical Report AFRL-OSR-VA-TR-2013-0134, CUBRC, 2013.

[16] C Running, TJ Juliano, JS Jewell, MP Borg, and RL Kimmel. Hypersonic shock-wave/boundary-layer interactions on a cone/flare. *Experimental Thermal and Fluid Science*, 109:109911, 2019.

[17] JG Marvin, JL Brown, and PA Gnoffo. Experimental database with baseline cfd solutions: 2-d and axisymmetric hypersonic shock-wave/turbulent-boundary-layer interactions. Technical Report NASA TM-2013-216604, NASA Ames, 2013.

[18] P Gnoffo. Validation studies for hypersonic flow prediction. In *39th aerospace sciences meeting and exhibit*, page 1025, 2001.

[19] IA Bedarev, AA Maslov, AA Sidorenko, NN Fedorova, and AN Shiplyuk. Experimental and numerical study of a hypersonic separated flow in the vicinity of a cone-flare model. *Journal of applied mechanics and technical physics*, 43:867–876, 2002.

[20] S Tissera, D Drikakis, and T Birch. Computational fluid dynamics methods for hypersonic flow around blunted-cone-cylinder-flare. *Journal of Spacecraft and Rockets*, 47(4):563–570, 2010.

[21] S Tissera, V Titarev, and D Drikakis. Chemically reacting flows around a double-cone, including ablation effects. In *48th AIAA Aerospace Sciences Meeting Including the New Horizons Forum and Aerospace Exposition*, 2010.

[22] N Kianvashrad and D Knight. Simulation of hypersonic shock-wave–laminar-boundary-layer interaction on hollow cylinder flare. *AIAA journal*, 55(1):322–326, 2017.

[23] D Knight, N Kianvashrad, and MR Youssefi. Simulation of hypersonic shock wave laminar boundary layer interactions. In *11th Ankara International Aerospace Conference*, 2021.

[24] G Shoev, G Oblapenko, O Kunova, M Mekhonoshina, and E Kustova. Validation of vibration-dissociation coupling models in hypersonic non-equilibrium separated flows. *Acta Astronautica*, 144:147–159, 2018.

[25] PG Cross and MR West. Simulation of hypersonic flowfields using star-ccm+. Technical report, Naval Air Warfare Center Weapons Division, 2019.

[26] G Candler, I Nompelis, M-C Druguet, M Holden, T Wadhams, I Boyd, and W-L Wang. Cfd validation for hypersonic flight-hypersonic double-cone flow simulations. In *40th AIAA aerospace sciences meeting & exhibit*, page 581, 2002.

[27] M Holden, J Harvey, T Wadhams, and M MacLean. A review of experimental studies with the double cone and hollow cylinder/flare configurations in the lens hypervelocity tunnels and comparisons with navier-stokes and dsmc computations. In *48th AIAA Aerospace Sciences Meeting Including the New Horizons Forum and Aerospace Exposition*, page 1281, 2010.

[28] D Knight, J Longo, D Drikakis, D Gaitonde, A Lani, I Nompelis, B Reimann, and L Walpot. Assessment of cfd capability for prediction of hypersonic shock interactions. *Progress in Aerospace Sciences*, 48:8–26, 2012.

[29] GV Candler. Next-generation cfd for hypersonic and aerothermal flows. In *22nd AIAA Computational Fluid Dynamics Conference*, page 3048, 2015.

[30] D Knight, O Chazot, J Austin, MA Badr, G Candler, B Celik, D de Rosa, R Donelli, J Komives, A Lani, et al. Assessment of predictive capabilities for aerodynamic heating in hypersonic flow. *Progress in Aerospace Sciences*, 90:39–53, 2017.

[31] D Knight, H Yan, A Panaras, and A Zheltovodov. Rto wg 10-cfd validation for shock wave turbulent boundary layer interactions. In *40th AIAA Aerospace Sciences Meeting & Exhibit*, page 437, 2002.

[32] R Alviani. *Assessment of Wilcox $k-\omega$ Turbulence Model in Regions of Shock Wave Turbulent Boundary Layer Interaction*. PhD thesis, Rutgers, The State University of New Jersey, New Brunswick, NJ, October 2018.

[33] RA Alviani. *Assessment of Wilcox k-ω turbulence model in regions of shock-wave turbulent boundary-layer interaction*. PhD thesis, Rutgers The State University of New Jersey, School of Graduate Studies, 2018.

[34] C Horstman. Hypersonic shock-wave turbulent-boundary-layer interaction flows-experiment and computation. In *22nd Fluid Dynamics, Plasma Dynamics and Lasers Conference*, page 1760, 1991.

[35] CJ Roy and FG Blottner. Review and assessment of turbulence models for hypersonic flows. *Progress in Aerospace Sciences*, 42(7-8):469–530, 2006.

[36] MJ Wright, GV Candler, and D Bose. Data-parallel line relaxation method for the navier-stokes equations. *AIAA journal*, 36(9):1603–1609, 1998.

[37] MJ Wright, T White, and N Mangini. Data parallel line relaxation (dplr) code user manual: Acadia-version 4.01. 1. Technical report, 2009.

[38] FR Menter. Two-equation eddy-viscosity turbulence models for engineering applications. *AIAA journal*, 32(8):1598–1605, 1994.

[39] DC Wilcox. *Turbulence Modeling for CFD, 3rd edition*. DCW Industries, 2006.

[40] A Mazaheri, PA Gnoffo, CO Johnston, and B Kleb. Laura users manual: 5.3-48528. Technical report, 2010.

[41] PA Gnoffo. An upwind-biased, point-implicit relaxation algorithm for viscous, compressible perfect-gas flows. Technical report, 1990.

[42] P Gnoffo, S Berry, and J Van Norman. Uncertainty assessments of 2d and axisymmetric hypersonic shock wave-turbulent boundary layer interaction simulations at compression corners. In *42nd AIAA thermophysics conference*, page 3142, 2011.

[43] N Georgiadis and D Yoder. Recalibration of the shear stress transport model to improve calculation of shock separated flows. In *51st AIAA Aerospace Sciences Meeting Including the New Horizons Forum and Aerospace Exposition*, page 685, 2013.

[44] PR Spalart. Strategies for turbulence modelling and simulations. *International journal of heat and fluid flow*, 21(3):252–263, 2000.

[45] MS Holden. Experimental research and analysis in supersonic and hypervelocity flows in the lens shock tunnels and expansion tunnel. In *20th AIAA international space planes and hypersonic systems and technologies conference*, page 3660, 2015.

[46] T Wadhams, M Holden, and M MacLean. Comparison of experimental and computational results from¢ blind£ turbulent shock wave interaction study over cone flare and hollow cylinder flare configuration. *AIAA Aviation. Atlanta, GA*, 2014.

[47] S Roy and K Sinha. Variable turbulent prandtl number model applied to hypersonic shock/boundary-layer interactions. In *2018 Fluid Dynamics Conference*, page 3728, 2018.

[48] S Roy and K Sinha. Turbulent heat flux model for hypersonic shock–boundary layer interaction. *AIAA Journal*, 57(8):3624–3629, 2019.

[49] K Sinha, K Mahesh, and GV Candler. Modeling shock unsteadiness in shock/turbulence interaction. *Physics of fluids*, 15(8):2290–2297, 2003.

[50] K Sinha, K Mahesh, and GV Candler. Modeling the effect of shock unsteadiness in shock/turbulent boundary-layer interactions. *AIAA journal*, 43(3):586–594, 2005.

[51] DK Prabhu. Shock wave interactions: A cfd study of cubrc lens-ii turbulent experiments. In *AIAA Aviation and Aeronautics Forum and Exposition*, number ARC-E-DAA-TN15585, 2014.

[52] A Ali Pasha, KA Juhany, and M Khalid. Numerical prediction of shock/boundary-layer interactions at high mach numbers using a modified spalart–allmaras model. *Engineering Applications of Computational Fluid Mechanics*, 12(1):459–472, 2018.

[53] DD Knight and G Degrez. Shock wave boundary layer interactions in high mach number flows a critical survey of current numerical prediction capabilities. *AGARD Advisory Report Agard Ar*, 2:1–1, 1998.

[54] D Knight, H Yan, AG Panaras, and A Zheltovodov. Advances in cfd prediction of shock wave turbulent boundary layer interactions. *Progress in Aerospace Sciences*, 39(2-3):121–184, 2003.

[55] WYK Chan, PA Jacobs, and DJ Mee. Suitability of the k–ω turbulence model for scramjet flowfield simulations. *International Journal for Numerical Methods in Fluids*, 70(4):493–514, 2012.

[56] H Zhang, TJ Craft, and H Iacovides. The formulation of the rans equations for supersonic and hypersonic turbulent flows. *The Aeronautical Journal*, 125(1285):525–555, March 2021.

[57] P Raje and K Sinha. Anisotropic SST turbulence model for shock-boundary layer interaction. *Computers & Fluids*, 228:105072, October 2021.

[58] A Wagner, JM Schramm, K Hannemann, R Whitside, and JP Hickey. Hypersonic shock wave boundary layer interaction studies on a flat plate at elevated surface temperature. In Konstantinos Kontis, editor, *Shock Wave Interactions*, pages 231–243, Cham, 2018. Springer International Publishing.

[59] C Prasad and DV Gaitonde. Turbulence modeling of 3d high-speed flows with upstream-informed corrections. *Shock Waves*, 33(2):99–115, March 2023.

[60] X Xiao, HA Hassan, JR Edwards, and RL Gaffney. Role of turbulent prandtl numbers on heat flux at hypersonic mach numbers. *AIAA Journal*, 45(4):806–813, April 2007.

[61] S Roy, U Pathak, and K Sinha. Variable turbulent prandtl number model for shock/boundary-layer interaction. *AIAA Journal*, 56(1):342–355, 2018.

[62] T Coakley and P Huang. Turbulence modeling for high speed flows. In *30th Aerospace Sciences Meeting and Exhibit*, page 436, 1992.

[63] CL Rumsey. Compressibility considerations for kw turbulence models in hypersonic boundary-layer applications. *Journal of Spacecraft and Rockets*, 47(1):11–20, 2010.

[64] G Tu, X Deng, and M Mao. Assessment of two turbulence models and some compressibility corrections for hypersonic compression corners by high-order difference schemes. *Chinese Journal of Aeronautics*, 25(1):25–32, 2012.

[65] TJ Coakley, CC Horstman, JG Marvin, JR Viegas, JE Bardina, PG Huang, and MI Kussoy. Turbulence compressibility corrections. Technical report, 1994.

[66] JJ Hoste. Assessment of scale resolving turbulence models in the TAU code for canonical shock-turbulence interaction. Technical Report DLR-FB-2020-28. 169 S, DLR, 2023.

[67] FR Menter, M Kuntz, and R Langtry. Ten years of industrial experience with the sst turbulence model. *Turbulence, heat and mass transfer*, 4(1):625–632, 2003.

[68] R Baurle. Modeling of high speed reacting flows: established practices and future challenges. In *42nd AIAA aerospace sciences meeting and exhibit*, page 267, 2004.

[69] F Génin and S Menon. Studies of shock/turbulent shear layer interaction using large-eddy simulation. *Computers and Fluids*, 39(5):800–819, 2010.

[70] R Quadros, K Sinha, and J Larsson. Turbulent energy flux generated by shock/homogeneous-turbulence interaction. *Journal of Fluid Mechanics*, 796:113–157, 2016.

[71] Amjad A. PASHA and Khalid A. JUHANY. Numerical simulation of compression corner flows at mach number 9. *Chinese Journal of Aeronautics*, 33(6):1611–1624, 2020.

[72] JB Vemula and K Sinha. Reynolds stress models applied to canonical shock-turbulence interaction. *Journal of Turbulence*, 18(7):653–687, 2017.

[73] S Karl, JP Hickey, and F Lacombe. Reynolds stress models for shock-turbulence interaction. In *31st International Symposium on Shock Waves 1: Fundamentals 31*, pages 511–517. Springer, 2019.

[74] JB Vemula and K Sinha. Explicit algebraic reynolds stress model for shock-dominated flows. *International Journal of Heat and Fluid Flow*, 85:108680, 2020.

[75] GA Gerolymos, Emilie Sauret, and I Vallet. Oblique-shock-wave/boundary-layer interaction using near-wall reynolds-stress models. *AIAA journal*, 42(6):1089–1100, 2004.

[76] N Kianvashrad and D Knight. Simulation of hypersonic shock wave-laminar boundary layer interactions. *Progress in Flight Physics–Volume 9*, 9:409–420, 2017.

[77] Siemens Digital Industries Software. Simcenter STAR-CCM+, version 2210. https://www.plm.automation.siemens.com/global/en/products/simcenter/STAR-CCM.html, Siemens 2022.

[78] S Langer, A Schwöppe, and N Kroll. The dlr flow solver tau - status and recent algorithmic developments. 2014.

[79] Y Wada and MS Liou. An accurate and robust flux splitting scheme for shock and contact discontinuities. *SIAM Journal on Scientific Computing*, 18(3):633–657, 1997.

[80] B van Leer. Towards the ultimate conservative difference scheme. v. a second-order sequel to godunov's method. *Journal of Computational Physics*, 32(1):101–136, 1979.

[81] B. Thornber, A. Mosedale, D. Drikakis, D. Youngs, and R.J.R. Williams. An improved reconstruction method for compressible flows with low mach number features. *Journal of Computational Physics*, 227(10):4873–4894, 2008.

[82] I Huismann, S Fechter, and T Leicht. Hypercoda–extension of flow solver coda to hypersonic flows. *HyperCODA–Extension of Flow Solver CODA Towards Hypersonic Flows*, 13, 2020.

[83] I Huismann, S Fechter, and T Leicht. Hypercoda–extension of flow solver coda towards hypersonic flows. In *New Results in Numerical and Experimental Fluid Mechanics XIII: Contributions to the 22nd STAB/DGLR Symposium*, pages 99–109. Springer, 2021.

[84] S Fechter and I Huismann. Hypercoda – extension of flow solver coda towards rocket flows. In *2022 9th European Conference for Aerospace Sciences (EUCASS)*, 2022.

[85] C Amato, S Fechter, I Huismann, and T Ecker. Application of hypercoda to hypersonic flows around two-dimensional geometries. In *HiSST 2024,3rd International Conference on High-Speed Vehicle Science and Technology*, 2024.

[86] SR Allmaras and FT Johnson. Modifications and clarifications for the implementation of the Spalart-Allmaras turbulence model. In *Seventh international conference on computational fluid dynamics (ICCFD7)*, volume 1902. Big Island, HI, 2012.

[87] S Chen, F Cai, H Xue, N Wang, and C Yan. An improved AUSM-family scheme with robustness and accuracy for all mach number flows. *Applied Mathematical Modelling*, 77:1065–1081, 2020.

[88] NN Gibbons, KA Damm, PA Jacobs, and RJ Gollan. Eilmer: An open-source multi-physics hypersonic flow solver. *Computer Physics Communications*, 282(108551), 2023.

[89] DC Wilcox. Formulation of the kw turbulence model revisited. *AIAA journal*, 46(11):2823–2838, 2008.

[90] KA Damm, NN Gibbons, and RJ Gollan. Application of a jacobian-free newton-krylov method to the simulation of hypersonic flows. In *AIAA SCITECH 2023 Forum*, number 2023-2295, National Harbor, MD & Online, January 2023.

[91] BJ McBride, MJ Zehe, and S Gordon. Nasa glenn coefficients for calculating thermodynamic properties of individual species. Technical Report 211556, National Aeronautics and Space Administration, 2002.

[92] B Mallol, M Boogaard, N Delsate, and C Hirsch. New meshing methods for ship propellers and hydrofoils. In *24th Numerical Towing Tank Symposium Proceedings*, pages 77–82, 2022.

[93] S Monté, L Temmerman, B Tartinville, B Léonard, and C Hirsch. Towards a separation sensitive explicit algebraic reynolds stress rans model. In *Ercoftac Bulletin 121*, pages 61–66. ERCOFTAC, 2019.

[94] E Lemmon, R Jacobsen, S Penoncello, and D Friend. Thermodynamic properties of air and mixtures of nitrogen, argon, and oxygen from 60 to 2000 k at pressures to 2000 mpa. *Journal of Physical and Chemical Reference Data - J PHYS CHEM REF DATA*, 29:331–385, 05 2000.

[95] V Driest. The problem of aerodynamic heating. In *Aerodynamic Heating: Aerodynamic Aspects Session Proceedings*, pages 26–41, 1956.

[96] TD Economon, F Palacios, SR Copeland, T Lukaczyk, and JJ Alonso. Su2: An open-source suite for multiphysics simulation and design. *AIAA Journal*, 54(3):828–846, 2016.

[97] WT Maier, JT Needels, C Garbacz, F Morgado, JJ Alonso, and M Fossati. Su2-nemo: An open-source framework for high-mach nonequilibrium multi-species flows. *Aerospace*, 8(7), 2021.

[98] SE Kim, S Mathur, J Murthy, and D Choudhury. A reynolds-averaged navier-stokes solver using unstructured mesh-based finite-volume scheme. In *36th AIAA Aerospace Sciences Meeting and Exhibit*, page 231, 1998.

[99] SE Kim and B Makarov. An implicit fractional-step method for efficient transient simulation of incompressible flows. In *17th AIAA Computational Fluid Dynamics Conference*, page 5253, 2005.

[100] JM Weiss, JP Maruszewski, and WA Smith. Implicit solution of preconditioned navier-stokes equations using algebraic multigrid. *AIAA journal*, 37(1):29–36, 1999.

[101] JM Weiss and WA Smith. Preconditioning applied to variable and constant density flows. *AIAA journal*, 33(11):2050–2057, 1995.

[102] FR Menter, A Matyushenko, and R Lechner. Development of a generalized k-ω two-equation turbulence model. In *New Results in Numerical and Experimental Fluid Mechanics XII: Contributions to the 21st STAB/DGLR Symposium, Darmstadt, Germany, 2018*, pages 101–109. Springer, 2020.